Hybrid InGaAsP-InP Mach-Zehnder Racetrack Resonator for Thermooptic Switching and Coupling Control

William M. J. Green, Reginald K. Lee, Guy A. DeRose, Axel Scherer, and Amnon Yariv

Electrical Engineering and Applied Physics, California Institute of Technology, 1200 East California Boulevard, M/C 136-93, Pasadena, California 91125, USA

wgreen@caltech.edu

Abstract: An InGaAsP-InP optical switch geometry based on electrical control of waveguide-resonator coupling is demonstrated. Thermooptic tuning of a Mach-Zehnder interferometer integrated with a racetrack resonator is shown to result in switching with ON-OFF contrast up to 18.5 dB. The optical characteristics of this unique design enable a substantial reduction of the switching power, to a value of 26 mW in comparison with 40 mW for a conventional Mach-Zehnder interferometer switch. Modulation response measurements reveal a 3 dB bandwidth of 400 kHz and a rise time of 1.8 μs, comparing favorably with current state-of-the-art thermooptic switches.

OCIS codes: (250.0250) Optoelectronics; (230.4110) Modulators

References and links

1. P. P. Absil, J. V. Hryniewicz, B. E. Little, R. A. Wilson, L. G. Joneckis, and P.-T. Ho, "Compact microring notch filters," IEEE Photon. Technol. Lett. **12**, 398–400 (2000).
2. B. E. Little, S. T. Chu, and H. A. Haus, "Track changing by use of the phase response of microspheres and resonators," Opt. Lett. **23**, 894–896 (1998).
3. J. E. Heebner and R. W. Boyd, "Enhanced all-optical switching by use of a nonlinear fiber ring resonator," Opt. Lett. **24**, 847–849 (1999).
4. R. W. Boyd and J. E. Heebner, "Sensitive disk resonator photonic biosensor," Appl. Opt. **40**, 5742–5747 (2001).
5. S. Blair and Y. Chen, "Resonant-enhanced evanescent-wave fluorescence biosensing with cylindrical optical cavities," Appl. Opt. **40**, 570–582 (2001).
6. M. T. Hill, H. J. S. Dorren, T. de Vries, X. J. M. Leijtens, J. H. den Besten, B. Smalbrugge, Y.-S. Oei, H. Binsma, G.-D. Khoe, and M. K. Smit, "A fast low-power optical memory based on coupled micro-ring lasers," Nature **432**, 206–209 (2004).
7. T. A. Ibrahim, W. Cao, Y. Kim, J. Li, J. Goldhar, P.-T. Ho, and C. H. Lee, "All-optical switching in a laterally coupled microring resonator by carrier injection," IEEE Photon. Technol. Lett. **15**, 36–38 (2003).
8. T. J. Kippenberg, S. M. Spillane, D. K. Armani, and K. J. Vahala, "Ultralow-threshold microcavity Raman laser on a microelectronic chip," Opt. Lett. **29**, 1224–1226 (2004).
9. B. E. Little, S. T. Chu, P. P. Absil, J. V. Hryniewicz, F. G. Johnson, F. Seiferth, D. Gill, V. Van, O. King, and M. Trakalo, "Very high-order microring resonator filters for WDM applications," IEEE Photon. Technol. Lett. **16**, 2263–2265 (2004).
10. A. Yariv, "Critical coupling and its control in optical waveguide-ring resonator systems," IEEE Photon. Technol. Lett. **14**, 483–485 (2002).
11. A. Yariv, "Universal relations for coupling of optical power between microresonators and dielectric waveguides," Electron. Lett. **36**, 321–322 (2000).
12. A. Yariv, in *Optical Electronics in Modern Communications*, 5th ed. (Oxford University Press, New York, 1997).
13. R. L. Espinola, M.-C. Tsai, J. T. Yardley, and R. M. Osgood, "Fast and low-power thermooptic switch on thin silicon-on-insulator," IEEE Photon. Technol. Lett. **15**, 1366–1368 (2003).

#6380 - $15.00 US Received 21 January 2005; revised 23 February 2005; accepted 24 February 2005

14. C. H. Lee, P. S. Mak, and A. P. DeFonzo, "Optical control of millimeter-wave propagation in dielectric waveguides," IEEE J. Quantum Electron. **16**, 277–288 (1980).
15. L. B. Soldano and E. C. M. Pennings, "Optical multi-mode interference devices based on self-imaging: principles and applications," J. Lightwave Technol. **13**, 615–627 (1995).
16. W. M. J. Green, J. Scheuer, G. A. DeRose, A. Yariv, and A. Scherer, "Assessment of lithographic process variation effects in InGaAsP annular Bragg resonator lasers," J. Vac. Sci. Technol. B **22**, 3206–3209 (2004).
17. L. A. Coldren and S. W. Corzine, in *Diode Lasers and Photonic Integrated Circuits* (Wiley-Interscience Publications, New York, 1995).
18. J. M. Choi, R. K. Lee, and A. Yariv, "Ring fiber resonators based on fused-fiber grating add-drop filters: application to resonator coupling," Opt. Lett. **27**, 1598–1600 (2002).

1. Introduction

Planar microring and microdisk resonators have been utilized in numerous linear and non-linear optical applications in recent years. The long photon storage times achieved by the high quality factor (Q) whispering-gallery modes in such resonators result in many technologically useful characteristics, including narrow-band filter response [1], highly non-linear phase response [2], and large cavity enhancement of the electric field [3]. These characteristics have been used to implement a wide range of devices, including biochemical sensors [4, 5], all-optical switches [6, 7], and low-threshold silica Raman lasers [8]. Furthermore, high index contrast waveguide materials have been used to realize microring and microdisk resonators with ultra-compact form, facilitating dense integration of these components into larger-scale functional photonic systems [9].

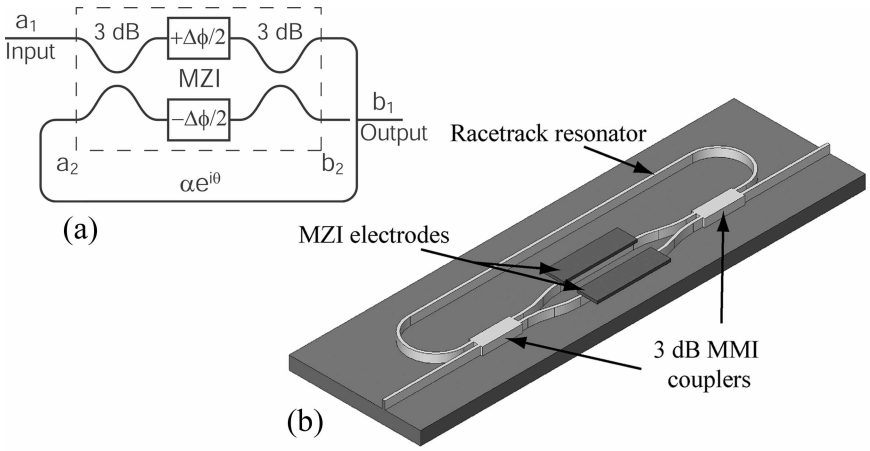

Fig. 1. Hybrid MZI/racetrack resonator switch schematic drawings. (a) Illustration of relevant electric field components and relative phase between arms of MZI. (b) Illustration of the device geometry as fabricated (not to scale). The planar fabrication process utilized requires that the output waveguides of the MZI be uncrossed, in contrast to the crossed configuration shown in (a).

One intriguing application of the microring resonator optical platform is the active control of an optical signal through precise command of the magnitude of waveguide-resonator coupling [10]. Consider the geometry in Fig. 1(a), in which one of the output ports of a 2×2 Mach-Zehnder interferometer (MZI) is connected with one of the input ports to form a racetrack-shaped resonator. In this composite architecture, the waveguide-resonator coupling coefficient κ can be modulated via electrical control of the relative phase $\Delta\phi$ between the MZI arms. It

#6380 - $15.00 US Received 21 January 2005; revised 23 February 2005; accepted 24 February 2005

has been shown that this hybrid MZI/racetrack resonator can achieve high-contrast modulation of an optical input wave, and furthermore, can reduce the required electrical switching power in comparison with a conventional MZI [10]. Switching is achieved by tuning $\Delta\phi$ to bring the resonator in and out of *critical coupling*, the state in which complete destructive interference occurs between the portion of the travelling wave coupled out of the resonator and the wave transmitted past the resonator [11]. In this work, we demonstrate an InGaAsP-InP semiconductor hybrid MZI/racetrack resonator switch, and achieve electrical control of waveguide-resonator coupling using thermooptic effects. This device exhibits the predicted reduction in switching power compared with a conventional MZI, good ON-OFF switching contrast, and microsecond switching speed.

The body of this paper is divided as follows. Section 2 presents a theoretical analysis of the hybrid switch's transmission characteristics, and quantifies the expected reduction in switching power in terms of the racetrack resonator loss. The fabrication of the InGaAsP-InP switch is discussed in Section 3. The steady-state optical transmission, modulation response, and rise time of the device are characterized in Section 4, and performance is compared to theoretical predictions. Finally, conclusions are presented in Section 5.

2. Theory

The optical transmission characteristics of the hybrid MZI/racetrack resonator switch in Fig. 1(a) are derived using the coupling matrix in Eq. (1), and the resonator circulation condition in Eq. (2) [10].

$$\begin{bmatrix} b_1 \\ b_2 \end{bmatrix} = \begin{bmatrix} t & \kappa \\ \kappa^* & -t^* \end{bmatrix} \begin{bmatrix} a_1 \\ a_2 \end{bmatrix} = i \begin{bmatrix} \cos(\Delta\phi/2) & -\sin(\Delta\phi/2) \\ \sin(\Delta\phi/2) & \cos(\Delta\phi/2) \end{bmatrix} \begin{bmatrix} a_1 \\ a_2 \end{bmatrix} \tag{1}$$

$$a_2 = \alpha e^{i\theta} b_2 \tag{2}$$

The coupling matrix relates the MZI input electric field components a_1 and a_2 to the MZI output components b_1 and b_2, through the coupling and transmission coefficients κ and t. Equation (1) shows that κ and t are functions of the relative phase $\Delta\phi$ between the arms of the MZI. For a lossless MZI, $|\kappa|^2 + |t|^2 = 1$. Light propagation through the resonator is characterized by a round-trip transmissivity α, and a phase factor $e^{i\theta}$, as shown in Eq. 2. For a lossless resonator, $\alpha = 1$. The round-trip phase is given by $\theta = 2\pi n_{eff} L_r/\lambda$, where n_{eff} is the effective index of the optical mode in the racetrack, L_r is the racetrack circumference, and λ is the optical wavelength. Combining these relationships results in the expression for the normalized transmitted optical power P_{out}/P_{in} shown in Eq. (3).

$$\frac{P_{out}}{P_{in}} = \left|\frac{b_1}{a_1}\right|^2 = \frac{\alpha^2 + \cos^2(\Delta\phi/2) - 2\alpha|\cos(\Delta\phi/2)|\cos(\theta)}{1 + \alpha^2\cos^2(\Delta\phi/2) - 2\alpha|\cos(\Delta\phi/2)|\cos(\theta)} \tag{3}$$

On resonance ($\theta = 2m\pi$, $m = 1, 2, 3...$), the normalized transmission becomes

$$\frac{P_{out}}{P_{in}} = \left|\frac{b_1}{a_1}\right|^2 = \frac{[\alpha - |\cos(\Delta\phi/2)|]^2}{[1 - \alpha|\cos(\Delta\phi/2)|]^2}. \tag{4}$$

Transmission through the device is switched from unity at $\Delta\phi = 0$ ($|t| = |\cos(\Delta\phi/2)| = 1$) to a theoretical value of zero at the condition of critical coupling, given by $\alpha = |t| = |\cos(\Delta\phi/2)|$, or $\Delta\phi = 2\cos^{-1}(\alpha)$. In contrast, the normalized transmission of a conventional MZI (one without an integrated resonator, equivalent to $\alpha = 0$) is given by $P_{out,MZI}/P_{in,MZI} = \cos^2(\Delta\phi/2)$, and the relative phase required for ON-OFF switching is $\Delta\phi = \pi$. Figure 2 compares the on-resonance normalized transmission through the hybrid device with that of a conventional MZI,

#6380 - $15.00 US Received 21 January 2005; revised 23 February 2005; accepted 24 February 2005

as a function of the relative phase $\Delta\phi$. For a low loss resonator as shown ($\alpha = 0.99$), the portion of the hybrid device's transmission curve near $\Delta\phi = 0$ is extremely steep. Compared with the conventional MZI, operation within this region makes high-contrast modulation possible with a comparatively small change in the relative phase $\Delta\phi$.

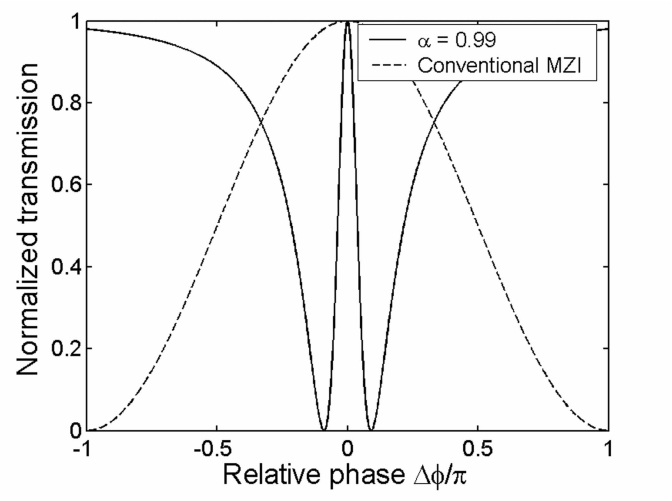

Fig. 2. Comparison of the on-resonance normalized transmission through the hybrid MZI/racetrack resonator switch with $\alpha = 0.99$, with the transmission through a conventional MZI. The hybrid device switches ON-OFF with a fraction of the π phase shift required for the conventional MZI.

In practical devices, it is possible to control $\Delta\phi$ electronically, through the application of an electric field or current. For example, electrooptic [12], thermooptic [13], or free carrier dispersion [14] effects may be utilized to control $\Delta\phi$. The reduction in the phase shift required for ON-OFF switching shown in Fig. 2 then translates into a reduction in the required applied voltage or electrical power. In the context of the thermooptic effects relevant to this work, it is appropriate to express the relative phase in terms of the dissipated electrical power ΔP_e (which induces a relative temperature change ΔT between the two arms of the MZI), as shown in Eq. (5).

$$\Delta\phi = \frac{\pi}{\Delta P_\pi}\Delta P_e \tag{5}$$

In the above expression, ΔP_π is defined as the power required to induce $\Delta\phi = \pi$, and is thus equivalent to the switching power for a conventional MZI. Therefore, critical coupling occurs when $\Delta P_e = \Delta P_{cr} = 2\Delta P_\pi \cos^{-1}(\alpha)/\pi$. The ratio of the switching powers $\Delta P_{cr}/\Delta P_\pi$, given in Eq. 6, provides a quantitative metric for comparison of the hybrid switch with the conventional MZI.

$$\frac{\Delta P_{cr}}{\Delta P_\pi} = \frac{2\cos^{-1}(\alpha)}{\pi} \tag{6}$$

Since the racetrack resonator transmissivity satisfies $0 \leq \alpha \leq 1$, this ratio is always less than unity, and can become very small in the limit of low resonator loss, $\alpha \sim 1$.

For the purposes of this analysis, it has been convenient to consider the switch as drawn in Fig 1(a), with the MZI output ports crossed. However, this crossed geometry is not physically realizable using the standard planar fabrication process employed in this work. Figure 1(b) shows the device as fabricated, with the MZI output ports uncrossed. The performance of the

#6380 - $15.00 US Received 21 January 2005; revised 23 February 2005; accepted 24 February 2005

uncrossed geometry follows directly from the analysis presented above, by simply exchanging $\Delta\phi$ with $\Delta\phi + \pi$.

3. Device fabrication

The hybrid switch geometry fabricated and tested is shown in Fig. 1(b). The MZI is composed of two 3 dB multimode interference (MMI) couplers [15] 8 μm wide and 90 μm long, and the MZI electrodes are 180 μm long. The racetrack resonator has bends of 50 μm radius, and a total circumference of 1430 μm. The single-mode channel waveguides are nominally 1.5 μm wide.

The InGaAsP-InP semiconductor waveguide structure consists of an n-type InP substrate, a 3 μm InP buffer/lower cladding layer, a 0.4 μm InGaAsP (λ_{gap} = 1.3 μm) waveguide core layer, a 1.2 μm InP upper cladding layer, and a 0.2 μm p-type InGaAs cap layer. The waveguide core and upper/lower cladding layers are grown nominally undoped, by metal-organic chemical vapor deposition (MOCVD). Fabrication of the device proceeds as follows. First, an etch mask layer of SiO_2 is deposited by plasma enhanced chemical vapor deposition (PECVD). A layer of poly(methyl methacrylate) (PMMA) electron beam resist is then applied by spin coating. Subsequently, direct electron beam lithography is employed to expose an array of patterns within the PMMA, using a Leica Microsystems EBPG 5000+ electron beam writer operating at 100 keV. After development, the PMMA patterns are transferred into the underlying SiO_2 layer using an inductively coupled plasma reactive ion etch (ICP-RIE) step and C_4F_8 gas. The remaining PMMA is removed using an O_2 plasma. Transfer of the patterns into the semiconductor substrate is accomplished using ICP-RIE etching and $HI/H_2/Ar$ chemistry [16], using the SiO_2 layer as a hard mask. The InGaAsP-InP waveguides are etched through the waveguide core to a depth of $\sim$3 μm, ensuring strong optical confinement for compact waveguide bends. The remaining SiO_2 mask is then removed in a buffered hydrofluoric acid solution. Next, a benzocyclobutene (BCB) electrical isolation layer is applied by spin coating and cured at 300 $^\circ$C. During the thermal cure, the BCB layer reflows and planarizes the sample surface. In a self-aligned procedure, a short ICP-RIE etch using a NF_3/O_2 gas mixture is used to partially etch back the BCB, exposing the tops of the waveguide ridges. Contact pads consisting of Cr/AuZn/Au are deposited on the MZI arms, using UV optical lithography and lift-off metallization. The InP substrate is mechanically thinned to a thickness of $\sim$100 μm, metallized on the back side with AuGe/Au, cleaved into bars, and mounted to brass submounts with conductive epoxy for testing.

4. Experiment and results

Light from a tunable laser source is coupled into the input waveguide facet of the switch through a 60x (NA = 0.65) aspheric lens. A 40x (NA = 0.55) aspheric lens is used to collect the transmitted light from the output end of the device. A calibrated optical power meter is placed at the output to measure the transmitted power. The polarization of the laser input is controlled with a set of fiber paddles and a linear polarizer. Active control of the switch is achieved through injection of current into one of the MZI electrodes shown in Fig. 1(b).

As discussed in Section 2, switching of the transmitted optical power is achieved through control of the coupling coefficient κ, via electrical modulation of the MZI relative phase $\Delta\phi$. The mechanism of phase control used here is thermooptic in nature. As current injected into the MZI electrode passes vertically through the series resistance of the semiconductor channel waveguide (measured at $\sim$600 Ω) and into the back side contact, ohmic heating changes the waveguide's refractive index, and introduces a phase shift given by

$$\Delta\phi = \frac{2\pi L_e}{\lambda}\frac{dn_{eff}}{dT}\Delta T = \frac{2\pi L_e}{\lambda}\frac{dn_{eff}}{dT}Z_T\Delta P_e, \tag{7}$$

#6380 - $15.00 US Received 21 January 2005; revised 23 February 2005; accepted 24 February 2005

where L_e is the electrode length, λ is the optical wavelength, dn_{eff}/dT is the waveguide's thermooptic coefficient, and ΔT is the temperature change [13]. In going from the first to the second equality in Eq. 7, the proportionality of the temperature change to the dissipated electrical power is expressed, where the proportionality constant Z_T is the thermal impedance [17]. The thermooptic coefficient is $dn_{eff}/dT \sim 2.7 \times 10^{-4}$ K^{-1}, as determined through a series of measurements observing the temperature-dependent spectral shift of a characteristic Fabry-Perot transmission spectrum, from waveguide Fabry-Perot cavities fabricated on the same InGaAsP-InP substrate.

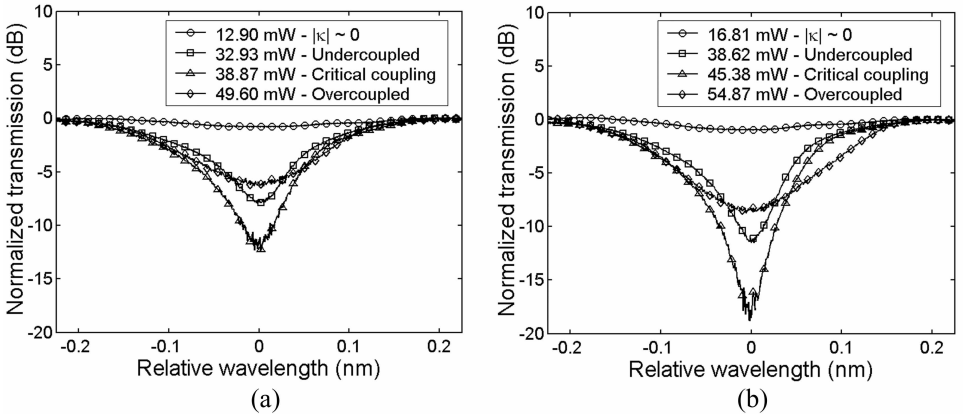

Fig. 3. Normalized transmission illustrating the behavior of a single racetrack resonance as the MZI is tuned. The electrical power dissipated in a single MZI electrode appears in the legend. (a) TE polarized input, maximum contrast ∼12 dB, switching power ∼ 26 mW. (b) TM polarized input, maximum contrast ∼18.5 dB, switching power ∼ 29 mW.

Figure 3 contains a portion of the switch's normalized transmission spectrum near λ = 1569 nm, plotted as a function of the electrical power dissipated within a single MZI electrode. The 0.45 nm wavelength span shown corresponds to one free spectral range of the racetrack resonator. Transmission is shown for TE polarized input in Fig. 3(a), and for TM polarization in Fig. 3(b). When the MZI is biased such that the magnitude of the coupling coefficient $|\kappa|$ is approximately zero, the transmission can be rendered relatively flat across the spectral region shown. As $|\kappa|$ is increased by further increasing the electrical power, the waveguide-resonator system is tuned through undercoupled, critically coupled, and overcoupled conditions. These conditions are characterized by the coupling coefficient being less than, equal to, or greater than the round-trip resonator loss, respectively [18]. On resonance, a contrast ratio of approximately 12 dB and 18.5 dB is observed near critical coupling, for TE and TM polarizations, respectively. The lower extinction observed for TE polarization is likely due to a slight polarization-dependent deviation from the ideal 50%/50% power splitting ratio in the MMI 3 dB couplers. The spectral width of the transmission null broadens as $|\kappa|$ increases with increasing electrical power, corresponding to the expected reduction in the loaded Q. From the linewidth at critical coupling, the unloaded intrinsic resonator Q is estimated to be 1.9×10^4 for TE and 1.7×10^4 for TM. The slight asymmetry seen in the lineshapes of the transmission minima in Fig. 3 is attributed to the influence of Fabry-Perot reflections from the cleaved facets of the device.

The switching power ΔP_{cr}, i.e., the power necessary to switch the hybrid device from the $|\kappa| \sim 0$ ($|t| \sim 1$) condition to critical coupling, is approximately 26 mW for TE and 29 mW for TM. By operating the MZI in the push-pull configuration, the switching power may be

#6380 - $15.00 US Received 21 January 2005; revised 23 February 2005; accepted 24 February 2005

further reduced by a factor of two. In comparison, conventional MZI modulators fabricated on the same substrate with identical electrode lengths are observed to have a (single electrode) switching power of $\Delta P_\pi \sim 40$ mW. Using Eq. 7 with $\Delta\phi = \pi$ gives a value of approximately 400 K/W for the thermal impedance Z_T. The observed reduction in switching power can be expressed following Eq. 6 as $(\Delta P_{cr}/\Delta P_\pi)_{\mathrm{TE}} = 0.65$, and $(\Delta P_{cr}/\Delta P_\pi)_{\mathrm{TM}} = 0.73$. This implies $\alpha_{\mathrm{TE}} \sim 0.52$, and $\alpha_{\mathrm{TM}} \sim 0.41$. Again, the lower switching power of the hybrid MZI/racetrack resonator switch compared to the conventional MZI is strictly due to the unique geometry for controlled waveguide-resonator coupling used here.

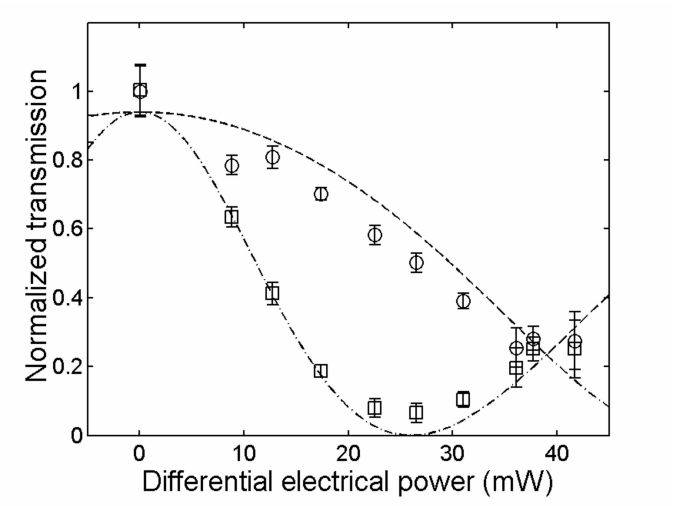

Fig. 4. Normalized transmission as a function of differential electrical power, for TE-polarized input. Square-marker data and dash-dotted guide-line represent on-resonance transmission. Circle-marker data and dashed guide-line indicate off-resonance transmission. Guide-lines are theoretical plots for $\alpha = 0.50$ and $\Delta P_\pi = 39$ mW.

Figure 4 plots the normalized transmission for TE-polarized input, both on-resonance (square markers, $\theta = 2m\pi$, $m = 1,2,3...$ in Eq. 3) and off-resonance (circle markers, $\theta = (2m-1)\pi$, $m = 1,2,3...$ in Eq. 3), as a function of the differential electrical power applied to a single MZI electrode. The power axis has been shifted by the power required to bias the hybrid switch to the state of maximum transmission. The error bars on the data account for uncertainty in the transmitted optical power, due to undesirable superimposed Fabry-Perot resonances from reflections at the cleaved facets of the device. The dash-dotted and dashed guide-lines are theoretical plots for the on-resonance and off-resonance transmission, respectively, with $\alpha = 0.50$ and $\Delta P_\pi = 39$ mW, and can be seen to follow the trends in the data. These values are in reasonable agreement with $\alpha_{\mathrm{TE}} \sim 0.52$ and $\Delta P_\pi \sim 40$ mW as obtained above, and suggest that a reasonable estimate of α can be made using the measured switching power reduction ratio $\Delta P_{cr}/\Delta P_\pi$. The theoretical guide-lines fit the data best with a maximum normalized transmission of 0.94 at a differential electrical power of zero, suggesting that the MZI itself may have some additional losses, i.e. $|\kappa|^2 + |t|^2 < 1$. These additional losses, as well as the relatively low values of α suggested by the data, can be attributed to scattering losses in the racetrack resonator, and to free carrier loss from a non-optimal MZI electrode structure.

To investigate the small signal modulation response, the TE polarized input is tuned into resonance with a racetrack mode at λ = 1564.54 nm. One arm of the MZI is driven at a bias power of $\sim$30 mW, superimposed with a 0.12 mW average power sinusoidal signal from a

#6380 - $15.00 US Received 21 January 2005; revised 23 February 2005; accepted 24 February 2005

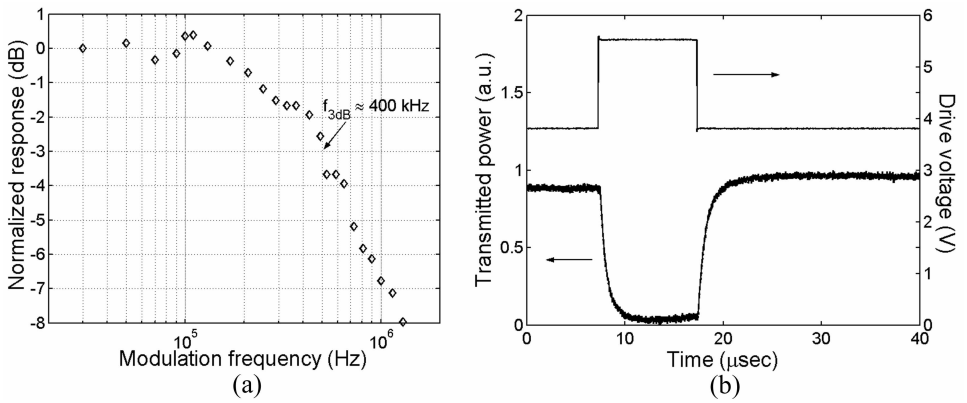

Fig. 5. (a) Frequency domain modulation response, showing 3 dB small-signal bandwidth of 400 kHz. (b) Temporal response of normalized optical transmission to a 10 μs voltage pulse, showing a rise/fall time of $\sim$1.8 μs.

function generator. The transmitted optical power is coupled into a single mode optical fiber and fed into a fast photodetector. A lock-in amplifier is used to extract the signal component at the modulation frequency, while this frequency is stepped from 30 kHz – 1.3 MHz. The resulting modulation response is plotted in Fig. 5(a), showing a 3 dB bandwidth of approximately 400 kHz. Figure 5(b) shows the time domain response to a 10 μs, 1.75 V peak-to-peak pulse. For the bias conditions shown, the positive-going voltage pulse gates the optical output into the OFF state by switching the hybrid MZI/resonator to the critical coupling condition. Fitting an exponential decay to the normalized transmission, a 10%-90% rise/fall time of $\sim$1.8 μs is extracted. In comparison with previous studies of integrated thermooptic switches, for example the silicon-on-insulator (SOI) MZI devices in [13], the InP-based hybrid switch presented here exhibits a $\sim$4x faster rise time and a switching power 60% smaller, while using a shorter thermooptic drive section. The improved performance is due to the unique hybrid design, in addition to enhanced thermal conductance in the InP structure.

The response time of the device can be improved dramatically by reduction of the large series resistance of the current path through the MZI waveguide. This can be achieved by inclusion of a p-i-n diode in the semiconductor epitaxy, and would permit fast free carrier dispersion effects [14] to become the dominant mechanism for control of the relative phase $\Delta\phi$.

5. Conclusion

In summary, a thermooptically tunable InGaAsP-InP MZI is used to electrically control the coupling coefficient to an integrated racetrack resonator. The resulting hybrid MZI/resonator geometry is demonstrated to tune through conditions of under, over, and critical coupling, and exhibits a maximum ON-OFF contrast ratio of 18.5 dB at critical coupling. A minimum switching power of 26 mW is measured for the hybrid device, while a conventional MZI fabricated for comparison is measured to require 40 mW for complete switching. These results demonstrate the reduction in switching power theoretically predicted for the hybrid MZI/resonator geometry. The switching power can be reduced by an additional factor of two by operating the MZI in push-pull mode. In addition, straightforward reduction of the racetrack resonator loss can result in further reduction of the switching power by as much as an order of magnitude [10]. Modulation response measurements reveal a rise time of 1.8 μs and a 3 dB modulation bandwidth of 400 kHz, illustrating that this coupling-controlled racetrack resonator architecture has

#6380 - $15.00 US Received 21 January 2005; revised 23 February 2005; accepted 24 February 2005

promise as a fast, low-power thermooptic switch. This switch may be easily integrated with other passive or thermally tunable InP-based devices, for compact photonic integrated systems.

Acknowledgment

The authors would like to thank Dr. Oskar Painter for providing access to fabrication facilities. In addition, John Choi, George Paloczi, Dr. Yanyi Huang, Dr. Koby Scheuer, and Dr. Tobias Kippenberg are thanked for their insightful comments and suggestions.

#6380 - $15.00 US Received 21 January 2005; revised 23 February 2005; accepted 24 February 2005